NANO LETTERS
Letter
Cite This: Nano Lett. 2018, 18, 7949−7954
pubs.acs.org/NanoLett

Nitrogen-Doped Carbon Nanotube Forests Planted on Cobalt Nanoflowers as Polysulfide Mediator for Ultralow Self-Discharge and High Areal-Capacity Lithium−Sulfur Batteries

Lianbo Ma,[†] Huinan Lin,[†] Wenjun Zhang,[†] Peiyang Zhao,[†] Guoyin Zhu,[†] Yi Hu,[†] Renpeng Chen,[†] Zuoxiu Tie,[†] Jie Liu,[†,‡] and Zhong Jin*[,†]

[†]Key Laboratory of Mesoscopic Chemistry of MOE, School of Chemistry and Chemical Engineering, Nanjing University, Nanjing, Jiangsu 210023, China

[‡]Department of Chemistry, Duke University, Durham, North Carolina 27708, United States

Supporting Information

ABSTRACT: Lithium−sulfur (Li−S) batteries with high theoretical energy density have caught enormous attention for electrochemical power source applications. However, the development of Li−S batteries is hindered by the electrochemical performance decay that resulted from low electrical conductivity of sulfur and serious shuttling effect of intermediate polysulfides. Moreover, the areal capacity is usually restricted by the low areal sulfur loadings (1.0−3.0 mg cm^{-2}). When the areal sulfur loading increases to a practically accepted level above 3.0−5.0 mg cm^{-2}, the areal capacity and cycling life tend to become inferior. Herein, we report an effective polysulfide mediator composed of nitrogen-doped carbon nanotube (N-CNT) forest planted on cobalt nanoflowers (N-CNTs/Co-NFs). The abundant pores in N-CNTs/Co-NFs can allow a high sulfur content (78 wt %) and block the dissolution/diffusion of polysulfides via physical confinement, and the Co nanoparticles and nitrogen heteroatoms (4.3 at. %) can enhance the polysulfide retention via strong chemisorption capability. Moreover, the planted N-CNT forest on N-CNTs/Co-NFs can enable fast electron transfer and electrolyte penetration. Benefiting from the above merits, the sulfur-filled N-CNTs/Co-NFs (S/N-CNTs/Co-NFs) cathodes with high areal sulfur loadings exhibit low self-discharge rate, high areal capacity, and stable cycling performance.

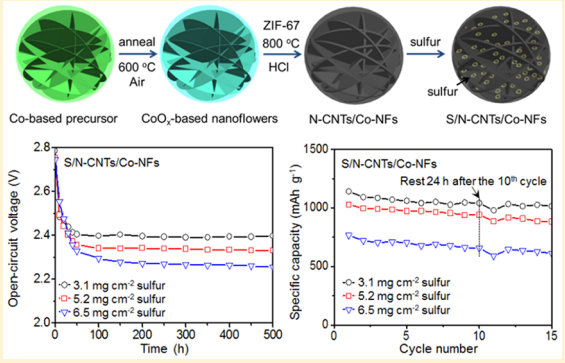

KEYWORDS: *Lithium−sulfur batteries, polysulfide mediator, high energy density, areal capacity, low self-discharge*

Lithium−sulfur (Li−S) batteries show great promise as next-generation energy storage devices owning to their high theoretical capacity (1675 mAh g^{-1}) and energy density (2600 Wh kg^{-1}),[1−3] which is about one order of magnitude greater than that of lithium-ion batteries (LIBs). Moreover, sulfur is nontoxic and reserve abundant in nature, and this enables Li−S batteries with better environmental friendliness and more attractive cost advantage compared to LIBs.[4,5] Unfortunately, besides these above merits, Li−S batteries also face several critical challenges including the low electrical conductivity and volume expansion of elemental sulfur, the easy dissolution of intermediate polysulfides, and most importantly, the low cycling stability.[6−8] Although strenuous efforts have been made to alleviate these issues, the achievements on improving the energy density of Li−S batteries are still severely limited.[9−16]

The simultaneous realization of high energy density and long cycling lifespan is always the very initial motivation of Li−S battery research.[17] However, in the present literature, the high specific gravimetric capacity or long cycling life batteries are often associated with low sulfur contents (usually ≤70.0 wt %) or low areal sulfur loadings (usually 1.0−3.0 mg cm^{-2}) in the cathodes, which make them less attractive for practical adoptions. Increasing the areal sulfur loadings in electrodes to improve the energy density of Li−S batteries would be an attractive solution. Nevertheless, the effective contact between electroactive sulfur and electrolyte would be significantly deteriorated, and also the serious self-discharge of batteries would unavoidably appear,[18] thus causing serious influence to the electrochemical performance, especially the capacity and cycling stability.[19−21] In this regard, it is crucial to achieve high energy density Li−S batteries under high areal sulfur loading (>5.0 mg cm^{-2}) accompanying with long cycling lifespan (more than 200 cycles) and low self-discharge rate.

Herein, we report the design of an effective polysulfide mediator composed of nitrogen-doped carbon nanotube (N-CNT) forest planted on cobalt nanoflowers (N-CNTs/Co-NFs), which can be used as an efficient sulfur host material for

Received: September 28, 2018
Revised: November 21, 2018
Published: November 30, 2018

DOI: 10.1021/acs.nanolett.8b03906
Nano Lett. 2018, 18, 7949−7954

Li−S batteries. The sulfur-mixed N-CNTs/Co-NFs (S/N-CNTs/Co-NFs) cathodes have micromesoporous structure and ultrahigh electrical conductivity, exhibiting strong chemisorption capability with sulfur species and electrocatalytic effect for polysulfide conversion. Moreover, the highly conductive channels of N-CNT forest decorated on the N-CNTs/Co-NFs can facilitate the fast electron transport and allow fluent electrolyte penetration, which are critically important to the electrochemical performance of Li−S batteries with high areal sulfur loadings. As a result, the S/N-CNTs/Co-NFs cathodes with very high areal sulfur loadings exhibit remarkably low self-discharge rate and stable cycling performance.

Results and Discussion. Figure 1a shows the detailed synthesis procedures of N-CNTs/Co-NFs and S/N-CNTs/Co-NFs. Starting with a hydrothermal method and followed by a thermal annealing process, flower-like CoO_x-based structure was synthesized. Then, through a chemical vapor deposition process under Ar/H_2 atmosphere with ZIF-67 as both the carbon and nitrogen sources,[22] Co nanocrystals were first formed and then served as the catalysts to promote the growth of N-CNT forest on the surface of flower-like structures. After chemical etching by using HCl solution (1.0 M), N-CNTs/Co-NFs material was successfully fabricated. Finally, through a typical melt-diffusion strategy for the loading of sulfur, the sulfur composite of S/N-CNTs/Co-NFs was prepared.

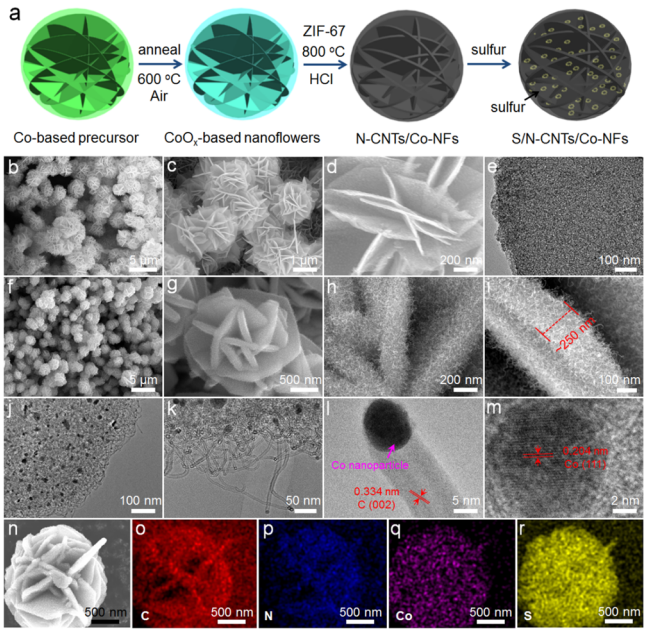

Figure 1. Synthesis process and microscopic characterizations of the samples. (a) Schematic synthesis approach of N-CNTs/Co-NFs and S/N-CNTs/Co-NFs. (b−d) SEM and (e) TEM images of CoO_x-based nanoflowers. (f−i) SEM, (j, k) TEM, and (l, m) HRTEM images of N-CNTs/Co-NFs. (n) SEM image and (o−r) elemental mapping results of S/N-CNTs/Co-NFs.

Figure 1b−d show the morphology of CoO_x-based nanoflowers, which exhibits the typical hierarchical features. The CoO_x-based nanoflowers are composed of closely assembled nanoplatelets. The size of CoO_x-based nanoflowers is about 2−3 μm, and the thickness of CoO_x-based nanoplatelets is about 30 nm (Figure 1e). The surface of CoO_x-based nanoplatelets can facilitate the catalytic growth of N-CNT forest. Figure 1f−i display the scanning electron microscopy (SEM) images of as-prepared N-CNTs/Co-NFs. The N-CNTs/Co-NFs still maintains the original morphology of CoO_x-based nanoflowers (Figure 1g), while the surface of nanoplatelets became rougher and fluffy, owing to the growth of N-CNT forest. As supplied in Figure 1h and i, the N-CNTs were grown in every directions, and the entire surface of nanoplatelets was covered by the densely grown N-CNT forest. As a result, the N-CNT forest was well planted onto Co-NFs, forming a superstructure with high stability and integrity. Transmission electron microscopy (TEM) was further conducted to study the structure features of N-CNTs/Co-NFs. Figure 1j and k present the typical TEM images of N-CNTs/Co-NFs, which reveal the porous nanostructure of N-CNT forest. The length of N-CNTs can reach several hundred nanometers, and the remaining Co catalyst nanoparticles (about 8−15 nm) underneath the N-CNTs can be clearly observed. The high-resolution TEM (HRTEM) image in Figure 1l discloses a lattice distance of 0.334 nm, corresponding to the (002) planes of N-CNTs, while the HRTEM image in Figure 1m reveals a lattice distance of 0.204 nm belonging to the (111) planes of metallic Co nanoparticle served as the catalyst for N-CNTs growth. Figure 1n−r display the typical SEM images of S/N-CNTs/Co-NFs after the loading of sulfur and the corresponding elemental mapping results. As illustrated, the S/N-CNTs/Co-NFs in Figure 1n maintains the initial morphology of N-CNTs/Co-NFs, and no aggregated sulfur particle was observed on the surface. The elemental mapping results (Figure 1o−r) show the presence of C, N, Co, and S elements, demonstrating the homogeneous distribution of sulfur in S/N-CNTs/Co-NFs.

The compositions and crystallinity of N-CNTs/Co-NFs and S/N-CNTs/Co-NFs were first studied by the XRD results. As shown in Figure 2a, the conspicuous peaks in the XRD pattern of N-CNTs/Co-NFs can be indexed into the metallic Co (JCPDS card, No. 89−4307). Moreover, a wide and weak peak (~25°) belonging to N-CNTs is also achieved. Besides these above diffraction peaks, S/N-CNTs/Co-NFs also exhibits the additional diffraction peaks of elemental sulfur. Raman

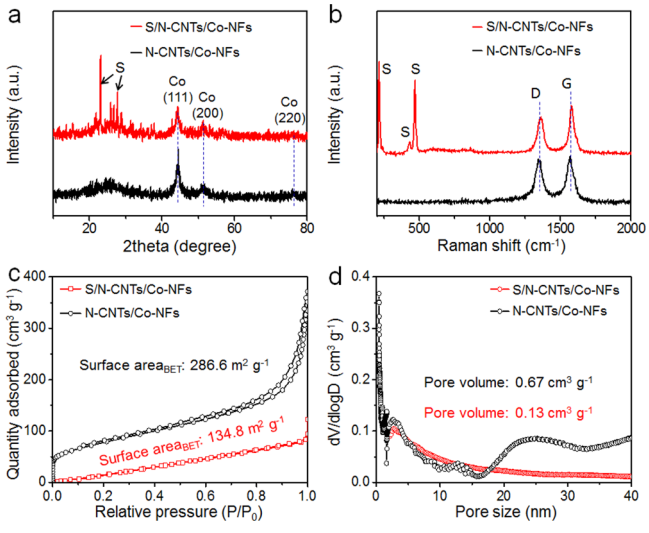

Figure 2. Structural characterizations of N-CNTs/Co-NFs and S/N-CNTs/Co-NFs. (a) XRD patterns, (b) Raman spectra, (c) N_2 adsorption−desorption isotherms, and (d) pore size distribution curves of N-CNTs/Co-NFs and S/N-CNTs/Co-NFs.

DOI: 10.1021/acs.nanolett.8b03906
Nano Lett. 2018, 18, 7949−7954

spectroscopy was conducted to identify the structural features of carbon and sulfur components. The Raman spectra of both N-CNTs/Co-NFs and S/N-CNTs/Co-NFs in Figure 2b display the typical D and G bands of carbonaceous materials. Moreover, S/N-CNTs/Co-NFs also exhibit the Raman peaks of elemental sulfur,[23] further indicating the preparation of sulfur composite. The specific surface area and pore size distribution of N-CNTs/Co-NFs before and after the loading of sulfur were investigated by N_2 adsorption−desorption measurements (Figure 2c,d). The N-CNTs/Co-NFs exhibits typical micromesoporous N_2 adsorption−desorption isotherms with a Brunauer−Emmett−Teller (BET) surface area of about 286.6 m^2 g^{-1}, and the pore volume reaches 0.67 cm^3 g^{-1}. The large number of micropores can adsorb polysulfides and alleviate the shuttling effect, while the mesopores can ensure the high loading content of sulfur and enhance the areal capacity.[24,25] After the loading of sulfur, the resultant S/N-CNTs/Co-NFs exhibits a greatly reduced BET surface area of 134.8 m^2 g^{-1}; meanwhile, the pore volume decreases dramatically to only 0.13 cm^3 g^{-1}.

The chemical states of S/N-CNTs/Co-NFs were further studied by X-ray photoelectron spectroscopy (XPS), as shown in Figure S1. The survey XPS spectrum of S/N-CNTs/Co-NFs (Figure S1a) reveals the presence of C, N, Co, and S elements, and the N content is measured to be about 4.3 at. %. The high-resolution XPS spectrum at N 1s region (Figure S1b) can be well fitted into three N species including pyridinic N (398.6 ± 0.2 eV), pyrrolic N (400.0 ± 0.2 eV), and graphitic N (401.1 ± 0.2 eV).[26] The pyridinic and pyrrolic N species can bond with sulfur species, thus enhancing the retention of polysulfides in Li−S batteries. By fitting the high-resolution XPS spectrum at S 2p region in Figure S1c, the chemical state of sulfur in S/N-CNTs/Co-NFs can be well understood. The S 2p XPS spectrum can be deconvoluted into two peaks, and the peaks at 163.7 and 164.7 eV belong to the S_8 molecules.[27,28] In addition, the accurate sulfur content in S/N-CNTs/Co-NFs was determined by thermogravimetric analysis (TGA) result under N_2 atmosphere from room temperature to 800 °C. As presented in Figure S2, owing to the large number of pores and high pore volume of N-CNTs/Co-NFs, the sulfur content in S/N-CNTs/Co-NFs can be as high as 78.0 wt %. When employed as sulfur cathode for Li−S batteries, the S/N-CNTs/Co-NFs with porous nanostructures, highly electrical conductive channels, and strong chemisorption capability with sulfur species can effective alleviate the issues caused by the low electrical conductivity of sulfur and the severe shuttle effect of polysulfides.

To investigate the effects of planted N-CNT forest on the electrochemical performances, a control sample was prepared with pure N_2 carrier gas instead of Ar/H_2 mixture. In this case, the control product is noted as carbon layer coated Co nanoflowers (CL/Co-NFs), which retains the initial flower-like morphology, but no N-CNTs were observed from the SEM images in Figure S3a, b. Moreover, the thickness of nanoplatelets on CL/Co-NFs increases due to the coating of carbon layer. The SEM image and corresponding elemental mapping results (Figure S3c-g) reveal the presence of C, N, and Co elements. After filling sulfur into CL/Co-NFs, the sulfur content in S/CL/Co-NFs determined by the TGA curve is 75.7 wt % (Figure S4). For better comparison, another control sample termed as S/CNTs was also prepared with commercial CNTs as the sulfur host. Figure S5a shows the typical SEM image of S/CNTs, which shows almost no sulfur particles on the surface, indicating the good result of sulfur filling. The corresponding XRD pattern reveals the coexistence of CNTs and elemental sulfur (Figure S5b). Additionally, the sulfur content in S/CNTs disclosed by the TGA curve reaches 68.8 wt % (Figure S5c).

The electrochemical performances of S/N-CNTs/Co-NFs as sulfur cathode were first evaluated in Li−S coin cells, with a normal areal sulfur loading of 1.0−1.5 mg cm^{-2}. For comparisons, the control samples of S/CL/Co-NFs and S/CNTs were also examined under the same experimental conditions. Figure 3a displays the galvanostatic charge/discharge profiles of S/N-CNTs/Co-NFs, S/CL/Co-NFs, and S/CNTs cathodes during the first cycle at 0.2 C. Each profile displays two discharge plateaus and one large charge plateau. The first discharge plateau is related to the reduction of S_8 to long-chain polysulfides (Li_2S_x, $4 \leq x \leq 8$), and the other discharge plateau corresponds to the further reduction from long-chain polysulfides to short-chain insoluble polysulfides (Li_2S_2 and Li_2S).[29,30] The single charge plateau suggests the one-step oxidation of short-chain polysulfides to elemental sulfur.[31−33] The initial discharge capacity of S/N-CNTs/Co-NFs cathode reaches 1262 mAh g^{-1}, higher than those of sulfur cathodes based on control samples. More importantly, the S/N-CNTs/Co-NFs cathode exhibits the longer and more stable discharge profile with much smaller potential polarizations compared to those of S/CL/Co-NFs and S/CNTs cathodes, further implying the electrocatalytic effect of N-CNTs/Co-NFs on polysulfide conversions.[34] The performance enhancement of N-CNTs/Co-NFs composite

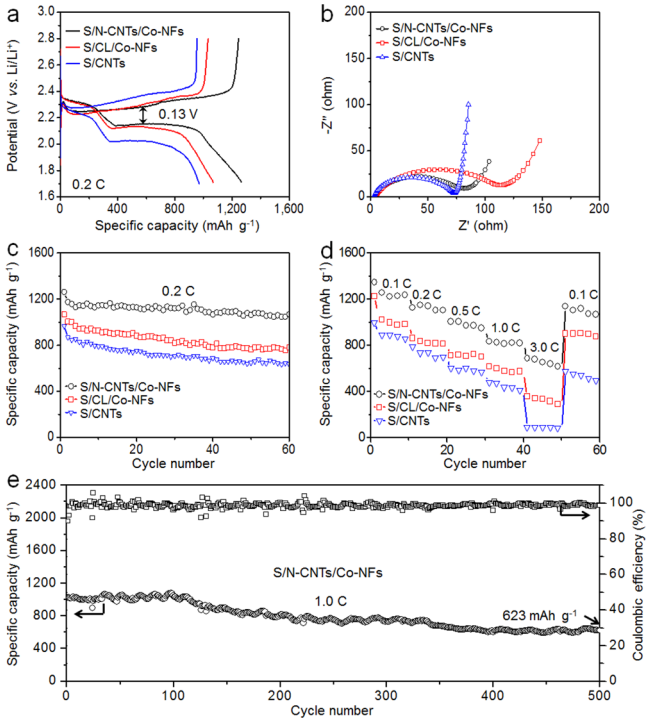

Figure 3. Electrochemical performances of S/N-CNTs/Co-NFs, S/CL/Co-NFs, and S/CNTs cathodes with the areal sulfur loading of 1.0−1.5 mg cm^{-2}. (a) Initial galvanostatic charge/discharge profiles, (b) Nyquist plots, (c) cycling performances, and (d) rate performances of S/N-CNTs/Co-NFs, S/CL/Co-NFs, and S/CNTs cathodes. (e) Long-term cycling performance and corresponding Coulombic efficiencies of S/N-CNTs/Co-NFs cathode at 1.0 C.

DOI: 10.1021/acs.nanolett.8b03906
Nano Lett. 2018, 18, 7949−7954

mainly originated from the synergistic effect of doped nitrogen heteroatoms and embedded Co nanoparticles.[35−39] The resistance characteristics of S/N-CNTs/Co-NFs, S/CL/Co-NFs, and S/CNTs cathodes were then investigated. As indicated by the electrochemical impedance spectroscopy (EIS) profiles in Figure 3b, the S/N-CNTs/Co-NFs cathode shows very low charge-transfer resistance, which is very conducive to the electrochemical performance.

Figure 3c compares the cycling performance of S/N-CNTs/Co-NFs, S/CL/Co-NFs, and S/CNTs cathodes at 0.2 C. The S/N-CNTs/Co-NFs cathode shows much better cycling stability within the initial 60 cycles. The discharge capacity of S/N-CNTs/Co-NFs cathode decreases to 1131 mAh g^{-1} at the fourth cycle, and then it keeps almost stable. A high discharge capacity of 1069 mAh g^{-1} is still achieved at the 60th cycle, corresponding to the high capacity retention of 84.7%. In contrast, the S/CL/Co-NFs and S/CNTs cathodes deliver much lower discharge capacities of only 782 and 637 mAh g^{-1} at the 60th cycle, respectively. The resistance characteristics of these sulfur cathodes after testing at 0.2 C were then investigated. As shown in Figure S6, all the sulfur cathodes exhibit the decreased charge-transfer resistances after cycling, further indicating the good charge transfer properties.

Figure 3d presents the rate performances of S/N-CNTs/Co-NFs, S/CL/Co-NFs, and S/CNTs cathodes under different current rates. With the better polysulfide retention capability, the S/N-CNTs/Co-NFs cathode shows higher specific capacities than other cathodes under the same current rates. Increasing the current rate from 0.1 C to 0.2, 0.5, 1.0, and 3.0 C, the specific capacities of S/N-CNTs/Co-NFs cathode decreases gradually from 1289 to 1140, 986, 847, and 684 mAh g^{-1}, respectively. However, for S/CL/Co-NFs and S/CNTs cathodes, the specific capacities decrease dramatically to 330 and 91 mAh g^{-1} at 3.0 C, respectively. These results demonstrate the much better rate capability of S/N-CNTs/Co-NFs cathode.

To further identify the cycling performance, the S/N-CNTs/Co-NFs cathode was tested for 500 cycles at 1.0 C. As shown in Figure 3e, the initial discharge capacity of S/N-CNTs/Co-NFs cathode reaches 1025 mAh g^{-1}, then it keeps stable during the initial 100 cycles, and finally a high reversible capacity of 623 mAh g^{-1} is achieved at the 500th cycle. This corresponds to the capacity retention of about 60.8%, accompanying with a low average capacity decay of 0.078% per cycle. Moreover, the Coulombic efficiency of S/N-CNTs/Co-NFs cathode after cycling 500 cycles at 1.0 C is approaching 100%, suggesting that the shuttle effect of polysulfides is well suppressed.[40−44] The excellent electrochemical performance of S/N-CNTs/Co-NFs based Li−S batteries should be attributed to the structural superiority of N-CNTs/Co-NFs composite. The Li−S batteries based on S/CL/Co-NFs and S/CNTs control samples were also investigated at 1.0 C (Figure S7) and exhibited much inferior cycling performances with the discharge capacities of only 239 and 109 mAh g^{-1} after 200 cycles, respectively. Moreover, compared with other representative sulfur cathodes in the literatures (Table S1),[14,31,45−54] S/N-CNTs/Co-NFs cathode also shows good electrochemical performance, demonstrating its potential as a promising sulfur host for Li−S batteries.

From the above electrochemical results, it can be seen that S/N-CNTs/Co-NFs cathodes show the much higher electrochemical performances than that of S/CL/Co-NFs cathodes. These improvements may be attributed to the following compositional and structural advantages of N-CNTs/Co-NFs: (1) the N-CNTs/Co-NFs composite has much higher electrical conductivity than that of CL/Co-NFs (Figure 3b), owing to the presence of N-CNT forest; (2) the N-CNT forest in N-CNTs/Co-NFs can serve as the mediator layer to store much amount of electrolyte and alleviate the shuttling of polysulfides, which is critical for the Li−S batteries with high areal sulfur loadings; (3) the Co nanocrystals remained on the tips of N-CNTs can facilitate the redox reactions of sulfur species, while for CL/Co-NFs, the Co nanoparticles were usually encapsulated by carbon layers, which restrict their electrocatalytic effect.

From a practical perspective on the research of Li−S batteries, it is critically important to construct novel cathode materials with high areal capacity and low self-discharge rate. Therefore, the self-discharge performance and cycling stability of the S/N-CNTs/Co-NFs cathodes under high areal sulfur loadings were investigated. Figure 4a shows the time-dependent open-circuit voltage profiles of Li−S batteries based on S/N-CNTs/Co-NFs cathodes with 3.1, 5.2, and 6.5 mg cm^{-2} sulfur, respectively. Under the sulfur loading of 3.1 mg cm^{-2}, the open-circuit voltage of S/N-CNTs/Co-NFs cathode was slowly dropped from 2.79 to 2.40 V after the standing time of 500 h. By increasing the sulfur loading to 5.2 mg cm^{-2}, the open-circuit voltage of S/N-CNTs/Co-NFs cathode only dropped from 2.75 to 2.33 V after storing for 500 h. Even at very high sulfur loading of 6.5 mg cm^{-2}, the open-circuit voltage of S/N-CNTs/Co-NFs cathode dropped from 2.75 to 2.26 V after 500 h. Thus, the open-circuit voltage decays of S/N-CNTs/Co-NFs cathodes with 3.1, 5.2, and 6.5 mg cm^{-2} sulfur are calculated to be 0.028%, 0.031%, and 0.036% per hour, respectively. Figure 4b displays the cycling performance of S/N-CNTs/Co-NFs cathodes with different areal sulfur loadings with the resting time of 24 h after the 10th cycle. After fully charged and stored for 24 h, the capacity losses at the 11th discharge step of the S/N-CNTs/Co-NFs cathodes with the sulfur loadings of 3.1, 5.2, and 6.5 mg cm^{-2}

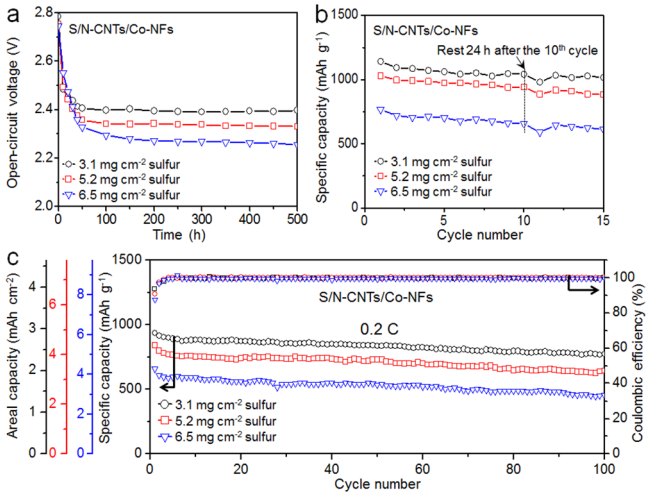

Figure 4. Electrochemical performances of S/N-CNTs/Co-NFs cathodes with high areal sulfur loadings. (a) Time-dependent open-circuit voltages of S/N-CNTs/Co-NFs cathodes with different areal sulfur loadings. (b) Self-discharge rate tests of S/N-CNTs/Co-NFs cathodes with different areal sulfur loadings with the standing time of 24 h after the 10th cycle at 0.1 C. (c) Cycling stability tests of S/N-CNTs/Co-NFs cathodes with different areal sulfur loadings (0.2 C).

DOI: 10.1021/acs.nanolett.8b03906
Nano Lett. 2018, 18, 7949−7954

are only 5.84%, 6.11%, and 10.2%, respectively. Moreover, the self-discharge rates of two control samples were also examined (Figure S8), exhibiting fast potential drop rates and high discharge capacity losses even under low areal sulfur loadings (9.8% for S/CL/Co-NFs and 11.4% for S/CNTs after storing for 24 h). All of these results indicate that the N-CNTs/Co-NFs can efficiently alleviate the self-discharge behavior of Li−S batteries.[17]

The cycling performances of S/N-CNTs/Co-NFs cathodes with various areal sulfur loadings at 0.2 C are displayed in Figure 4c. The initial discharge capacities of S/N-CNTs/Co-NFs cathodes with 3.1, 5.2, and 6.5 mg cm^{-2} sulfur are 936, 841, and 659 mAh g^{-1}, corresponding to the areal capacities of 2.90, 4.37, and 4.28 mAh cm^{-2}, respectively. The achieved highest areal capacity for S/N-CNTs/Co-NFs cathode is about 4.37 mAh cm^{-2}, which is relatively high among the reported sulfur cathodes in literature (Figure S9).[20,55−61] After 100 cycles, the discharge capacities of S/N-CNTs/Co-NFs cathodes with 3.1, 5.2, and 6.5 mg cm^{-2} sulfur slightly decreased to 772, 643, and 455 mAh g^{-1} (2.39, 3.34, and 2.96 mAh cm^{-2}), respectively, and the corresponding capacity retentions are 82.5%, 76.5%, and 69.0%. The achieved high electrochemical performance of S/N-CNTs/Co-NFs cathodes under high areal sulfur loadings can be attributed to the highly conductive network and smooth ion diffusion in the hierarchical nanostructure of N-CNTs/Co-NFs. The planted N-CNT forest provides conductive channels for fast electron transfer, and the flower-like architecture of N-CNTs/Co-NFs with large surface area and high porosity can maintain good contact interfaces with electrolyte. As a result, the S/N-CNTs/Co-NFs composite shows promising performances for high areal-capacity Li−S batteries.

Conclusions. In summary, here we propose the rational design and preparation of flower-like Co nanostructure with planted N-CNT forest as a promising sulfur host for Li−S batteries. Benefiting from the high electrical conductivity, abundant micromesopores, strong chemisorption capability with sulfur species, and electrocatalytic effect for polysulfide conversion, the S/N-CNTs/Co-NFs cathodes exhibit the very low self-discharge rate and stable cycling performance under high areal sulfur loadings. We expect this work may provide new insights for the construction of hybrid sulfur host materials to achieve high-performance Li−S batteries for practical utility.

■ ASSOCIATED CONTENT

Supporting Information

The Supporting Information is available free of charge on the ACS Publications website at DOI: 10.1021/acs.nanolett.8b03906.

Experimental section, Table S1, Figures S1−S9 (PDF)

■ AUTHOR INFORMATION

Corresponding Author

*E-mail: zhongjin@nju.edu.cn.

ORCID

Jie Liu: 0000-0003-0451-6111

Zhong Jin: 0000-0001-8860-8579

Notes

The authors declare no competing financial interest.

■ ACKNOWLEDGMENTS

This work is supported by National Key R&D Program of China (2017YFA0208200, 2016YFB0700600, 2015CB659300), Projects of NSFC (21872069, 51761135104, 21573108), Fundamental Research Funds for the Central Universities (020514380146), and High-Level Entrepreneurial and Innovative Talents Program of Jiangsu Province.

■ REFERENCES

(1) Wang, H. L.; Yang, Y.; Liang, Y. Y.; Robinson, J. T.; Li, Y. G.; Jackson, A.; Cui, Y.; Dai, H. *Nano Lett.* **2011**, *11*, 2644−2647.

(2) Yang, Y.; Zheng, G. Y.; Cui, Y. *Chem. Soc. Rev.* **2013**, *42*, 3018−3032.

(3) Xin, S.; Gu, L.; Zhao, N. H.; Yin, Y. X.; Zhou, L. J.; Guo, Y. G.; Wan, L. J. *J. Am. Chem. Soc.* **2012**, *134*, 18510−18513.

(4) Liang, C. D.; Dudney, N. J.; Howe, J. Y. *Chem. Mater.* **2009**, *21*, 4724−4730.

(5) Yin, Y. X.; Xin, S.; Guo, Y. G.; Wan, L. *Angew. Chem., Int. Ed.* **2013**, *52*, 13186−13200.

(6) Manthiram, A.; Fu, Y. Z.; Su, Y. S. *Acc. Chem. Res.* **2013**, *46*, 1125−1134.

(7) Evers, S.; Nazar, L. F. *Acc. Chem. Res.* **2013**, *46*, 1135−1143.

(8) Wang, J.; Yang, J.; Wan, C.; Du, K.; Xu, N.; et al. *Adv. Funct. Mater.* **2003**, *13*, 487−492.

(9) Ji, L. W.; Rao, M. M.; Zheng, H. M.; Zhang, L.; Li, Y. C.; Duan, W. H.; Guo, J. H.; Cairns, E. J.; Zhang, Y. G. *J. Am. Chem. Soc.* **2011**, *133*, 18522−18525.

(10) Su, Y. S.; Manthiram, A. *Nat. Commun.* **2012**, *3*, 1166.

(11) Li, W. Y.; Zhang, Q. F.; Zheng, G. Y.; Seh, Z. W.; Yao, H. B.; Cui, Y. *Nano Lett.* **2013**, *13*, 5534−5540.

(12) Wei Seh, Z.; Li, W. Y.; Cha, J. J.; Zheng, G. Y.; Yang, Y.; McDowell, M. T.; Hsu, P. C.; Cui, Y. *Nat. Commun.* **2013**, *4*, 1331.

(13) Wang, X. L.; Li, G.; Li, J. D.; Zhang, Y. N.; Wook, A.; Yu, A. P.; Chen, Z. W. *Energy Environ. Sci.* **2016**, *9*, 2533−2538.

(14) Li, Z.; Zhang, J. T.; Lou, X. W. *Angew. Chem., Int. Ed.* **2015**, *54*, 12886−12890.

(15) Seh, Z. W.; Yu, J. H.; Hsu, P. C.; Wang, H.; Sun, Y.; Yao, H.; Zhang, Q.; Cui, Y.; et al. *Nat. Commun.* **2014**, *5*, 5017.

(16) Chen, W.; Lei, T. Y.; Lv, W. Q.; Hu, Y.; Yan, Y. C.; Jiao, Y.; He, W. D.; Li, Z. H.; Yan, C. L.; Xiong, J. *Adv. Mater.* **2018**, *30*, 1804084.

(17) Fang, X.; Peng, H. S. *Small* **2015**, *11*, 1488−1511.

(18) Chung, S. H.; Manthiram, A. *ACS Energy Lett.* **2017**, *2*, 1056−1061.

(19) Li, Y. J.; Fu, K.; Chen, C. J.; Luo, W.; Gao, T. T.; Xu, S. M.; Dai, J. Q.; Pastel, G.; Wang, Y. B.; Liu, B. Y.; Song, J. W.; Chen, Y. N.; Yang, C. P.; Hu, L. B. *ACS Nano* **2017**, *11*, 4801−4807.

(20) Song, Y. Z.; Zhao, W.; Wei, N.; Zhang, L.; Ding, F.; Liu, Z. F.; Sun, J. Y. *Nano Energy* **2018**, *53*, 432−439.

(21) Lv, D.; Zheng, J.; Li, Q.; Xie, X.; Ferrara, S.; Nie, Z. M.; Mehdi, L. B.; Browning, N. D.; Zhang, J.; Graff, G.; Liu, J.; Xiao, J. *Adv. Energy Mater.* **2015**, *5*, 1402290.

(22) Li, Z. H.; Shao, M. F.; Yang, Q. H.; Tang, Y.; Wei, M.; Evans, D. G.; Duan, X. *Nano Energy* **2017**, *37*, 98−107.

(23) Lyu, Z. Y.; Xu, D.; Yang, L. J.; Che, R. C.; Feng, R.; Zhao, J.; Li, Y.; Wu, Q.; Wang, X. Z.; Hu, Z. *Nano Energy* **2015**, *12*, 657−665.

(24) Lee, J. S.; Kim, W.; Jang, J.; Manthiram, A. *Adv. Energy Mater.* **2017**, *7*, 1601943.

(25) Zheng, J. H.; Guo, G. N.; Li, H. W.; Wang, L.; Wang, B. W.; Yu, H. J.; Yan, Y. C.; Yang, D.; Dong, A. G. *ACS Energy Lett.* **2017**, *2*, 1105−1114.

(26) Ma, L. B.; Chen, R. P.; Hu, Y.; Zhu, G. Y.; Chen, T.; Lv, H. L.; Liang, J.; Tie, Z. X.; Jin, Z.; Liu, J. *Nanoscale* **2016**, *8*, 17911−17918.

(27) Zhang, Z.; Li, Z.; Hao, F.; Wang, X.; Li, Q.; Qi, Y.; Fan, R.; Yin, L. *Adv. Funct. Mater.* **2014**, *24*, 2500−2509.

(28) Mi, K.; Jiang, Y.; Feng, J.; Qian, Y.; Xiong, S. *Adv. Funct. Mater.* **2016**, *26*, 1571−1579.

DOI: 10.1021/acs.nanolett.8b03906
Nano Lett. 2018, 18, 7949−7954

(29) Zhang, Z.; Kong, L. L.; Liu, S.; Li, G. R.; Gao, X. P. *Adv. Energy Mater.* **2017**, *7*, 1602543.
(30) Su, D. W.; Cortie, M.; Wang, G. X. *Adv. Energy Mater.* **2017**, *7*, 1602014.
(31) Zhang, J.; Shi, Y.; Ding, Y.; Zhang, W. K.; Yu, G. H. *Nano Lett.* **2016**, *16*, 7276−7281.
(32) Lu, S. T.; Cheng, Y. W.; Wu, X. H.; Liu, J. *Nano Lett.* **2013**, *13*, 2485−2489.
(33) Zhou, G.; Zhao, Y.; Zu, C.; Manthiram, A. *Nano Energy* **2015**, *12*, 240−249.
(34) Ma, L. B.; Yuan, H.; Zhang, W. J.; Zhu, G. Y.; Wang, Y. R.; Hu, Y.; Zhao, P. Y.; Chen, R. P.; Chen, T.; Liu, J.; Hu, Z.; Jin, Z. *Nano Lett.* **2017**, *17*, 7839−7846.
(35) Ma, L. B.; Chen, R. P.; Zhu, G. Y.; Hu, Y.; Wang, Y. R.; Chen, T.; Liu, J.; Jin, Z. *ACS Nano* **2017**, *11*, 7274−7283.
(36) Chen, K.; Sun, Z. H.; Fang, R. P.; Shi, Y.; Cheng, H. M.; Li, F. *Adv. Funct. Mater.* **2018**, *28*, 1707592.
(37) Li, Z. Q.; Li, C. X.; Ge, X. L.; Ma, J. Y.; Zhang, Z. W.; Li, Q.; Wang, C. X.; Yin, L. W. *Nano Energy* **2016**, *23*, 15−26.
(38) Li, J. Y.; Fan, J. M.; Zheng, M. S.; Dong, Q. F. *Energy Environ. Sci.* **2016**, *9*, 1998−2004.
(39) Chen, T.; Cheng, B. R.; Zhu, G. Y.; Chen, R. P.; Hu, Y.; Ma, L. B.; Lv, H. L.; Wang, Y. R.; Liang, J.; Tie, Z. X.; Jin, Z.; Liu, J. *Nano Lett.* **2017**, *17*, 437−444.
(40) Yu, M. P.; Ma, J. S.; Xie, M.; Song, H. Q.; Tian, F. Y.; Xu, S. S.; Zhou, Y.; Li, B.; Wu, D.; Qiu, H.; Wang, R. M. *Adv. Energy Mater.* **2017**, *7*, 1602347.
(41) Ghosh, D.; Gad, M.; Lau, I.; Pope, M. A. *Adv. Energy Mater.* **2018**, *8*, 1801979.
(42) Peng, H. J.; Zhang, Z. W.; Huang, J. Q.; Zhang, G.; Xie, J.; Xu, W. T.; Shi, J. L.; Chen, X.; Cheng, X. B.; Zhang, Q. *Adv. Mater.* **2016**, *28*, 9551−9558.
(43) Xie, K. Y.; You, Y.; Yuan, K.; Lu, W.; Zhang, K.; Xu, F.; Ye, M.; Ke, S. M.; Shen, C.; Zeng, X. R.; Fan, X. L.; Wei, B. *Adv. Mater.* **2017**, *29*, 1604724.
(44) Liang, X.; Rangom, Y.; Kwok, C. Y.; Pang, Q.; Nazar, L. F. *Adv. Mater.* **2017**, *29*, 1603040.
(45) He, B.; Li, W. C.; Yang, C.; Wang, S. Q.; Lu, A. H. *ACS Nano* **2016**, *10*, 1633−1639.
(46) Zhong, Y.; Xia, X. H.; Deng, S. J.; Zhan, J. Y.; Fang, R. Y.; Xia, Y.; Wang, X. L.; Zhang, Q.; Tu, J. P. *Adv. Energy Mater.* **2018**, *8*, 1701110.
(47) Zhou, G. M.; Sun, J.; Jin, Y.; Chen, W.; Zu, C. X.; Zhang, R. F.; Qiu, Y. C.; Zhao, J.; Zhuo, D.; Liu, Y. Y.; Tao, X. Y.; Liu, W.; Yan, K.; Lee, H. R.; et al. *Adv. Mater.* **2017**, *29*, 1603366.
(48) Bao, W. Z.; Su, D. W.; Zhang, W. X.; Guo, X.; Wang, G. X. *Adv. Funct. Mater.* **2016**, *26*, 8746−8756.
(49) Ye, C.; Zhang, L.; Guo, C. X.; Li, D. D.; Vasileff, A.; Wang, H. H.; Qiao, S. Z. *Adv. Funct. Mater.* **2017**, *27*, 1702524.
(50) Liang, X.; Garsuch, A.; Nazar, L. F. *Angew. Chem., Int. Ed.* **2015**, *54*, 3907−3911.
(51) Li, Z.; Zhang, J. T.; Guan, B. Y.; Wang, D.; Liu, L. M.; Lou, X. W. *Nat. Commun.* **2016**, *7*, 13065.
(52) Ni, L. B.; Zhao, G. J.; Yang, G.; Niu, G. S.; Chen, M.; Diao, G. W. *ACS Appl. Mater. Interfaces* **2017**, *9*, 34793−34803.
(53) Zhu, Q. Z.; Zhao, Q.; An, Y. B.; Anasori, B.; Wang, H. R.; Xu, B. *Nano Energy* **2017**, *33*, 402−409.
(54) Xu, H. H.; Manthiram, A. *Nano Energy* **2017**, *33*, 124−129.
(55) Huang, S. Z.; Wang, Y.; Hu, J. P.; Lim, Y. V.; Kong, D. Z.; Zheng, Y.; Ding, M.; Pam, M. E.; Yang, H. Y. *ACS Nano* **2018**, *12*, 9504−9512.
(56) Gao, X. T.; Xie, Y.; Zhu, X. D.; Sun, K. N.; Xie, X. M.; Liu, Y. T.; Yu, J. Y.; Ding, B. *Small* **2018**, *14*, 1802443.
(57) Yu, Q. H.; Lu, Y.; Luo, R. J.; Liu, X. M.; Huo, K. F.; Kim, J. K.; He, J.; Luo, Y. S. *Adv. Funct. Mater.* **2018**, *28*, 1804520.
(58) Zhang, J. T.; Li, Z.; Chen, Y.; Gao, S. Y.; Lou, X. W. *Angew. Chem., Int. Ed.* **2018**, *57*, 10944−10948.
(59) Luo, L.; Chung, S. H.; Manthiram, A. *Adv. Energy Mater.* **2018**, *8*, 1801014.
(60) Li, G. R.; Lei, W.; Luo, D.; Deng, Y. P.; Deng, Z. P.; Wang, D. L.; Yu, A. P.; Chen, Z. W. *Energy Environ. Sci.* **2018**, *11*, 2372−2381.
(61) Bao, W. Z.; Liu, L.; Wang, C. Y.; Choi, S. H.; Wang, D.; Wang, G. X. *Adv. Energy Mater.* **2018**, *8*, 1702485.

DOI: 10.1021/acs.nanolett.8b03906
Nano Lett. 2018, 18, 7949−7954